



Small Block Model Tests for the Behaviour of a Blocky Rock Mass Under a Concentrated Rock Anchor Load

Bjarte Grindheim · Karsten Sannes Aasbø ·
Are Håvard Høyen · Charlie C. Li

Received: 8 April 2022 / Accepted: 15 July 2022
© The Author(s) 2022

Abstract Rock anchors are used to stabilise large-scale infrastructure such as the foundations of high buildings or road cuts, and their failure could lead to severe economic and social consequences. A rock anchor can fail in one or more of the following four modes; breakage of the tendon steel, tendon-grout bond failure, grout-rock bond failure and rock mass failure. In current rock anchor design, the knowledge for the first two failure modes is satisfactorily known and is relatively easy to test. The scientific background for the last two failure modes still has a potential of improvement and further development of the design criteria is needed. To help fill this gap, a series of block model tests were conducted on a small-scale test apparatus to evaluate the load capacity of a blocky mass under a rock anchor load. Digital image correlation (DIC) was used to monitor the full-field displacements in the block models. The tests showed that load arches were formed in the block layers and the anchor load was transferred to the side frames of the apparatus through these arches. The load capacity

of the mass increased with the number of the block layers and the confinement. The observed load arches and the effect of the confinement were also captured in a numerical model using UDEC software. The DIC monitoring showed that the displacements in the block model were identical along a vertical line. At a given depth, the displacements decrease with the distance to the centre line of the anchor.

Keywords Block model · Anchor pullout · Load distribution · Failure mode · Numerical modelling

1 Introduction

Rock anchors are used as load carrying elements for large-scale infrastructure by transferring large loads to the stable rock ground (Xanthakos 1991; Brown 2015). Anchors have been used for dam reinforcement (Xu and Benmokrane 1996; Cavill 1997), stabilisation of large structures (Jordan 2007; Koca et al. 2011), bridges (Schlotfeldt et al. 2013), reducing wind turbine foundation size (Yan et al. 2013; Shabanimashcool et al. 2018), reinforcement of underground caverns (Aoki 2007; Ma et al. 2021) and slopes (Choi et al. 2013; Wang et al. 2018), anchorage of submerged structures (Mothersille and Littlejohn 2012; Roesen and Trankjær 2021), and reinforcement of structures in seismic regions (Takemura et al. 2007).

B. Grindheim (✉) · K. S. Aasbø · C. C. Li
Department of Geoscience and Petroleum, NTNU,
Trondheim, Norway
e-mail: bjarte.grindheim@ntnu.no

K. S. Aasbø
Nordic Construction Company (NCC), Oslo, Norway

A. H. Høyen
Norwegian Public Roads Administration (NPRA), Bergen,
Norway

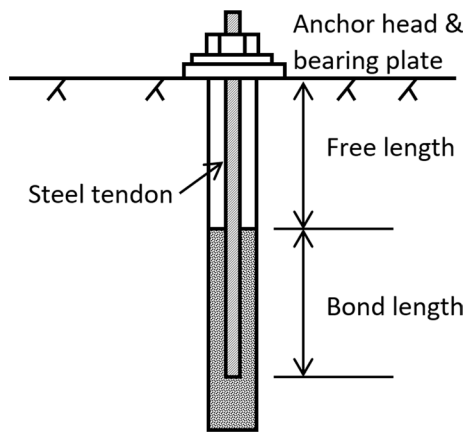


Fig. 1 Rock anchor components

A typical rock anchor is shown in Fig. 1. It consists of a steel tendon, which is stressed to transfer the loads from or fasten the structure to the ground. The ground around the anchor is stressed through shear loads from the anchor (Hanna 1982; Hobst and Zajíc 1983; Xanthakos 1991). Anchor loads are transferred to structures or rock surfaces through the anchor head. The end of the tendon is fastened to the ground through a bonded length. Between the anchor head and the bond length is the free length, which elongates freely during the tensioning (stressing) of the anchor.

There are four principal ways a rock anchor could fail. They are failure within the rock mass (Mode 1), failure of the grout-rock bond (Mode 2), failure of the tendon-grout bond (Mode 3), and failure of the steel tendon or anchor head (Mode 4) (Littlejohn and Bruce 1977). These failure modes are shown in Fig. 2. The ultimate tensile capacity of an anchor is the lowest load among the four failure modes (Kim and Cho 2012). When the failure modes are considered, they are usually calculated for individual anchors except for failure mode 1. Rock anchors are often installed in close proximity to each other, then it is important to account for the interaction between adjacent anchors when considering failure mode 1 (Brown 2015).

Earlier research has investigated rock anchors to some extent in the laboratory. The most common laboratory tests are anchor pullout tests. Failure mode 3, grout-tendon interface failure, has been tested, for example, by Barley (1997); Jarred and Haberfield (1997); Kim and Lee (2005); Ivanovic and Neilson

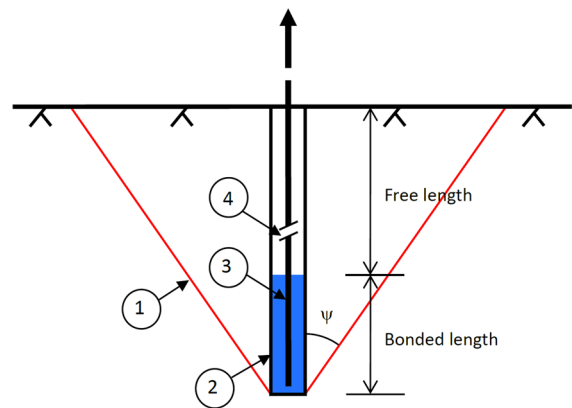


Fig. 2 The four principal failure modes of a grouted rock anchor under tension. (1) Rock mass uplift failure; (2) grout-rock bond or interface failure; (3) tendon-grout bond or interface failure; and (4) steel tendon tensile failure

(2008) and Akisanya and Ivanovic (2014). Barley (1997) also tested failure mode 2, grout-rock interface failure, when investigating the behaviour of grout in a confined state. García-Wolfrum et al. (2007) conducted pullout tests on intact rock samples to investigate conical failure (mode 1). Farmer (1975) and Benmokrane et al. (1995a) monitored the stresses along the tendon during pullout tests. Kaiser et al. (1992) investigated the effect stress changes had on the tendon-grout pullout/bond strength by changing the confining pressure around the bond length. Benmokrane et al. (1995b) studied the effect of grout on the pullout strength, while Jia et al. (2019) tried to optimise the grouting mixture and Park et al. (2013) tested different grouting methods. Zheng et al. (2016) developed a lab-model to investigate the performance of a rock anchor in a rock slope in a seismically active area, where the anchor was cyclically loaded.

The most similar tests to those reported in this paper was run by Dados (1984), who tested the pullout of an anchor in a block model. The blocks were made up of aluminium cubes and a confinement was set on the sides of the model. The test showed that the blocks bulged upward during the pullout test, and the vertical joints tended to open.

The design of rock anchors requires understanding of the mechanisms and interaction between the anchor and the surrounding rock (Showkati et al. 2015). A thorough review has been carried out by Brown (2015) on the design of post-tensioned anchors. The review concluded that the design is

based on simplified assumptions about the stress distribution, shape and volume of the rock influenced, and the failure mechanisms. The design was also considered to be excessively conservative and represents poor engineering practice. There is thus a clear need to increase knowledge about the stress distribution and how failure develops in the rock mass around a rock anchor.

In Norway, the ground rock mass is in general hard and massive, but contains fractures, geological discontinuities and foliation that sometimes function as weakness planes. These geological structures cut the rock to blocks in various sizes. Rock failure occurs often along the geological structures in such a blocky rock mass. Under the concentrated loading condition by a rock anchor, a load-arching effect may exist in the blocky rock mass, which would significantly enhance the load-bearing capacity of the rock mass. The current design practice only takes into account the dead weight or presumptive shear strength values of the potential failed rock body which results in underestimates of the load capacity of the rock mass. There are currently no specific guidelines for load estimation in blocky rock masses. It is therefore important to investigate how the load is transferred from an anchor to the blocky rock masses as well as the load capacity of the rock mass.

The objectives of this paper are to qualitatively demonstrate the deformation behaviour of rock blocks, the arching effect, and the failure mode of the blocky rock mass through laboratory pull tests on a specially designed mini test rig. Digital image correlation (DIC) was used to measure the displacements in the block models. UDEC modelling was also conducted after the model tests to verify the results of the

physical testing. Tests similar to those in this study have, to the best knowledge of the authors, not previously been carried out and therefore seem to be novel.

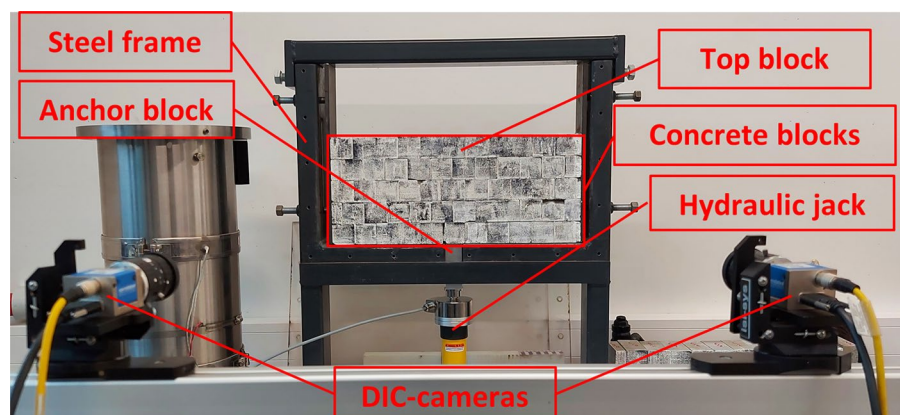
2 Physical Testing

2.1 Experimental Program

2.1.1 Mini Test Rig

The constructed test setup is shown in Fig. 3. The mini test rig consisted of a steel frame made of rectangular tubes and a hydraulic jack. There is an opening 4 cm × 10 cm in the middle of the bottom horizontal beam. A steel block representing the rock anchor goes through the opening and contacts the bottom layer of the blocks. The working area in the frame has dimensions 60 cm × 40 cm × 10 cm (width × height × depth). Concrete blocks are placed on the bottom frame in layers, to build up the blocky rock mass model. On each side of the frame there are two bolts which are tightened to provide lateral confinement to the model blocks. A steel plate is placed between the side blocks and the bolts to distribute the bolt load evenly (Fig. 4). A steel beam was fastened on top of the side frame pillars to enhance the horizontal stiffness of the frame. A manually operated hydraulic jack is used to apply the load to the anchor block. It is fastened to the bottom frame by two bolts and the load from the hydraulic jack is measured with a load cell. The movements of the blocks are measured by DIC technology with two cameras. It was a question how the anchor load would be applied in the model tests when the test setup was designed. As previously

Fig. 3 The mini test rig composed of a steel frame and hydraulic jack, and equipped with DIC cameras



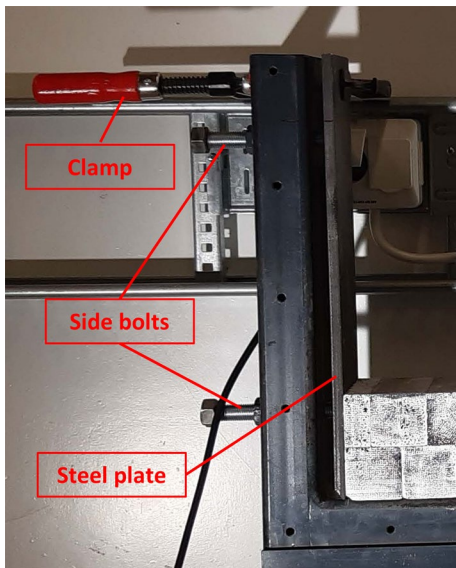


Fig. 4 Increased horizontal stiffness of steel plates with clamps

mentioned, the anchor load in reality is applied to the rock mass through the shear stress at the anchor-grout and grout-rock contacts. The purpose of this experimental study is the behaviour and failure mode of a blocky rock mass under a concentrated anchor load, but not the behaviour of the contacts. The effects will be the same regardless of whether the anchor load is applied by pull or compression, provided the directions of the loads on the rock anchor are the same. To simplify the loading procedure, therefore, it was decided to construct the setup so that the anchor load would be applied by pressing a rigid block upward in the bottom of the model.

Three models were run with increased stiffness, shown in Figs. 4 and 5. The stiffness was increased in two ways, with clamps on top of the steel plates in two models with two and three layers (Fig. 4), and with extra steel plates in the void between the frame and the steel plates in a model with five layers (Fig. 5).

2.1.2 Test Materials

The materials used in the test were 20 cm × 5 cm × 40 cm concrete pavement blocks. These were cut into small blocks with dimensions of 5 cm ×

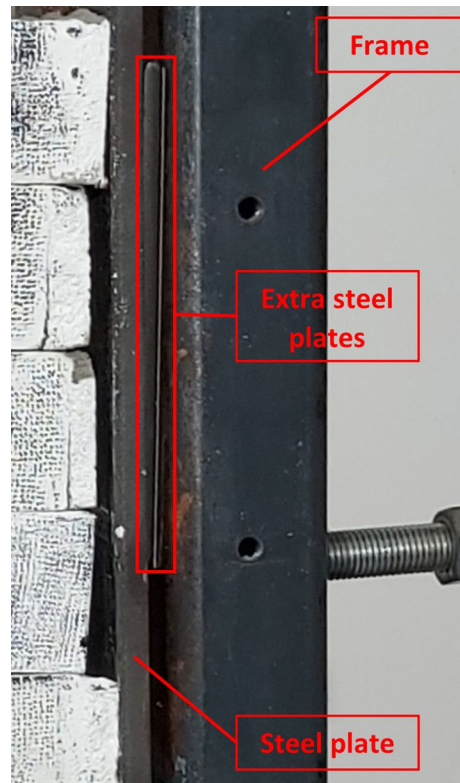


Fig. 5 Increased horizontal stiffness with extra steel plates in the void between the frame and steel plates

5 cm × 10 cm and 2.5 cm × 5 cm × 10 cm. Small errors occurred during cutting, which resulted in an uneven width of the block layers in the model. To ensure a satisfactory contact between each layer's end blocks and the side steel plate a cement liner (Fischer cement express) was used to fill the gaps.

Five 40 mm cores were drilled out of the concrete pavement blocks and cylindrical samples prepared. The samples were tested under uniaxial compression as described in Bieniawski and Bernede (1979) to obtain the mechanical properties of the concrete material. The axial and radial strains were measured during the tests to calculate the Young's modulus (E) and Poisson's ratio (ν). The uniaxial compressive strength (UCS/σ_c) was measured to 65.3 MPa, the Young's modulus 27.7 GPa and Poisson's ratio 0.25. The UCS was used to estimate the tensile strength (σ_t) and the cohesion (c) of the concrete using equations 1 (Indian Standard 2000) and 2 (Sivakugan et al. 2014):

$$\sigma_t = 0.7\sqrt{\sigma_c} \tag{1}$$

$$c = \frac{0.5\sigma_c\sigma_t}{\sqrt{\sigma_t(\sigma_c - 3\sigma_t)}} \tag{2}$$

From the equations, the tensile strength was estimated to be 5.66 MPa and the cohesion 11.2 MPa. Tu et al. (2020) found in their tests on high strength concrete (UCS > 60 MPa) that the friction angle (ϕ) of the concrete was 34°. This value was assumed to be representative for the concrete blocks. The basic friction angles of the blocks were also measured with tilt-tests (Fig. 6) as described in Alejano et al. (2018). Two basic friction angles were measured on the blocks, one on rough untreated surfaces and one on smoother cut surfaces: 41.2° for the rough surfaces and 31.3° for the cut surfaces.

2.1.3 DIC Monitoring

The tests were monitored with DIC cameras from Correlated Solutions. The side of the concrete blocks facing the cameras had to be painted white before a speckle pattern was applied on the surface. The speckle pattern was non-repetitive and was 50/50 black and white with high contrast. The speckles should have a size of at least 3–4 pixels to avoid aliasing (Correlated Solutions 2020). The cameras were placed at a distance where the whole block model could be seen with both cameras, and they had an angle of 25° between them. During the tests the loading was applied slowly with a load rate varying from 12–75 N/s, so the cameras were set to take two images per second (i.e., four images in total per second). The load rate was decided based on the operator



Fig. 6 Test apparatus used for the tilt-tests

trying applying loading in a steady and controlled manner but varied greatly due to the manual operation of the hydraulic jack. The software used to analyse the images post testing was Vic-3D (Correlated Solutions 2020). The strains were calculated from changes in the speckle pattern by taking reference in an image from before the tests started.

2.1.4 Estimation of Rock Mass Strength and Horizontal Confinement

In the design of rock anchors, the strength is commonly estimated based upon the weight of overlying rock and in some countries the shear or tensile strength of the rock mass is also included in the calculations, generally by applying assumed values of the tensile strength, shear strength and cohesion (Brown 2015). The strength of the block mass in the model was estimated with the design method based on the weight of overlying rock. This is a commonly applied method for estimating rock anchor strength against failure mode 1 in weak and heavily fractured rock masses (Brown 2015). The shape of the rock mass volume over the anchor is illustrated in Fig. 7. The anchor capacity was estimated using

$$Q_{cone} = \left[2 \cdot \frac{1}{2}h \cdot (h \cdot \tan \alpha) + d \cdot h \right] \cdot z \cdot \gamma \tag{3}$$

$$= (h^2 \cdot \tan \alpha + d \cdot h)z \cdot \gamma$$

where h is the height of the mobilised cone, α the angle of the potential failure cone, d the width of the

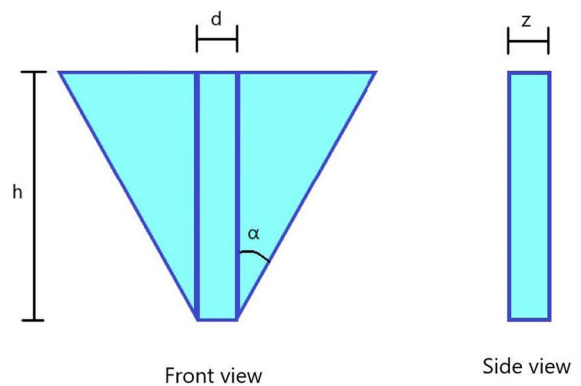


Fig. 7 Illustration of the dimensions of a hypothetical uplifted cone of rock mass, z illustrates the depth of the uplifted material

loaded block, z the depth of the model and γ the unit weight of the block material. In the tests, $h = 0.05$ m \times number of layers, $d = 0.05$ m, $z = 0.1$ m, and $\gamma = 22563$ N/m³. Based on the staggered pattern, $\alpha \approx 25^\circ$ (sect. 2.2.2). This results in an estimated capacity of 213 N for a model with 8 layers and 94 N for a model with 5 layers.

Confinement was applied to the model by applying torque to the bolts on the side of the model. The torque was applied with a torque wrench at 2.5–25 Nm. The numerical modelling of the tests required input of the confinement on the model, estimated based upon the applied torque with (USACE 1990):

$$T = P_B \cdot \left(\frac{L}{2\pi} + \frac{d_2 \cdot \mu_1}{2 \cos \alpha} + \frac{(d + b) \cdot \mu_2}{4} \right) \quad (4)$$

where T is the applied torque, P_B the resulting axial force in the bolt, L the lead of the thread helix, d_2 the pitch diameter of the bolt, μ_1 the coefficient of friction of the bolt thread, α the angle of the thread pitch, d the nominal bolt diameter (at the bolt head), and b the diameter of the washer face.

The equation was simplified since the bolt head did not interact with any other materials, and then both d and b could be set to zero. The bolt and the frame were made of steel and were lubricated with mineral oil which resulted in an approximate coefficient of friction μ_1 of 0.15 (USACE 1990). The bolt pitch diameter d_2 was 16 mm and the lead L of the thread helix was 2.0 mm. The angle of the thread pitch α was 60° . The calculated bolt force was then used to calculate the resulting stress on the side of the block mass with

$$S = \frac{2P_B}{A_{Bm}} \quad (5)$$

where S is the resulting stress in the side of the block mass, P_B the force applied by the bolts, and A_{Bm} the area of the block mass on the side. The estimated confinements are shown in Table 1.

2.1.5 Test Procedure

Several tests were run with the block model. The number of layers and confinement were varied. All the tests followed the same procedure, which is shown step by step here:

1. The blocks were placed in the model with the number of layers wanted.
2. Confinement was applied to the blocks by tightening the bolts on the sides.
3. The DIC cameras were calibrated.
4. The DIC capturing software was started.
5. The block model was then loaded gradually by the anchor block at the middle bottom. The loading was stopped when a desired load was reached or failure occurred.
6. The system was then unloaded slowly.
7. The DIC capturing was stopped.

2.2 Physical Testing Results

2.2.1 Load-Deformation Behaviour

The loading of the block model showed that the displacement at the anchor block and the displacement in the top centre block were almost equal. At small displacements, they were slightly larger in the anchor block, while with large displacements the top centre block had the greatest displacement due to bulging of the layers, as demonstrated in Fig. 8. Figure 9 shows the load-vertical displacement curve when the block model was run to failure. The curves show a linear relationship between the load and the displacement at small loads (elastic behaviour) then the curve starts to bend until a peak load is reached before the load starts to drop while the displacements increase (plastic deformation) until the model failed abruptly. The total displacement in the block models was reduced with increasing confinement and increasing number of layers, as demonstrated in Figs. 10–12. It was also observed that the vertical displacement was reduced when the horizontal stiffness of the steel plates was increased with clamps or adding extra steel plates, shown in Figs. 4 and 5. The results from the block model tests are summarised in Table 1.

2.2.2 Load Transfer in Rock Mass During External Loading

The load of the anchor block was transferred to the blocks in the middle of the bottom of the model. The displacements of the blocks were largest in the centre of the model at the bottom at small loads. They decreased upwards and at the sides. As an example,

Fig. 8 Plots of the load applied on the anchor block versus the vertical displacements of the anchor block (A) and the centre concrete block (TC) on the top layer in three typical model tests

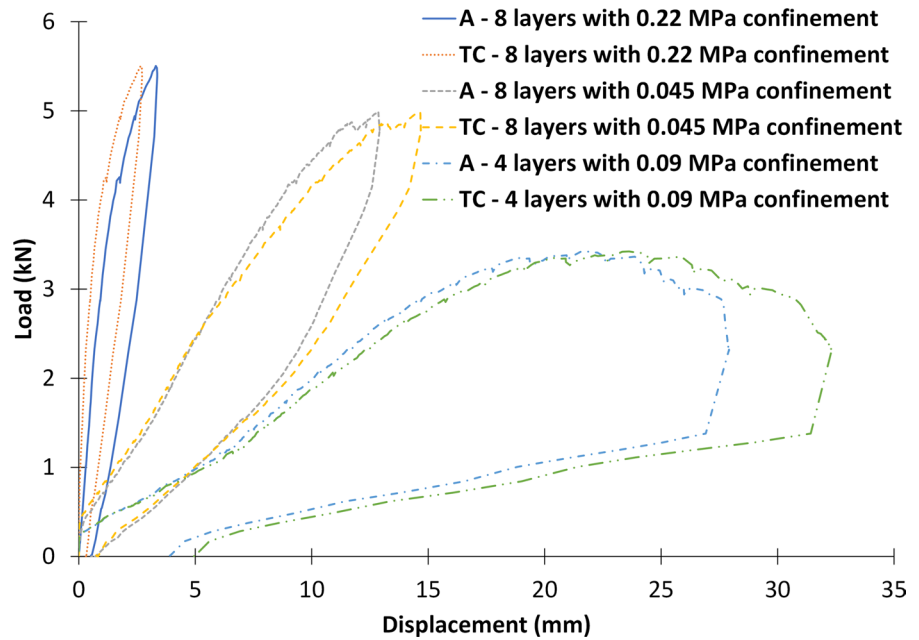


Fig. 9 Plots of the load applied on the anchor block versus the vertical displacements of the anchor block (A) and the centre concrete block (TC) on the top layer in the model test run to failure (test no. 9)

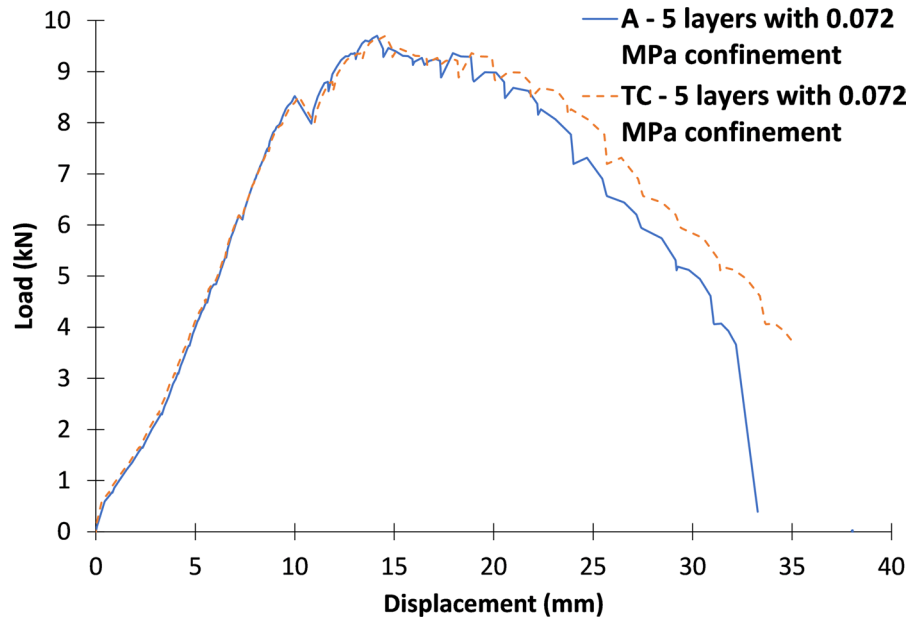


Fig. 13 shows the displacement of the model in test 1 at four different loads.

The horizontal strains in the material were processed with the DIC software Vic-3D. The blocks in the model rotated and bulged upwards during loading. Figure 14 shows the horizontal strains of the model in test 1 at Fig. 13 D with an applied load of 5.5 kN, and the potential failure cone (α)

based upon the fracture pattern. The vertical joints opened (red) at the top of the blocks in the middle of each layer and were pressed (purple) at the bottom. On the sides, the joints were pressed at the top and tended to open at the bottom. Apparently, a load arch, which is the trajectory of the most pressed portion of the joints, was formed in each layer. The load arches in each layer diverged the anchor

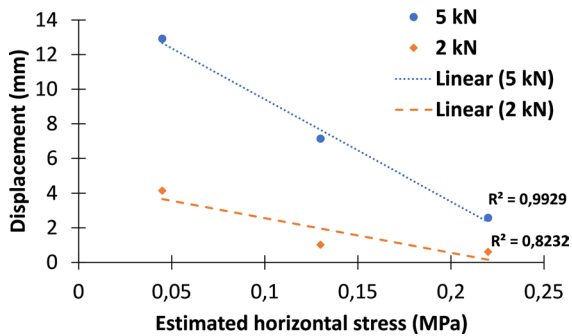


Fig. 10 Vertical displacement in models with 8 layers at 2 kN and 5 kN anchor load with trend lines

load to the frame of the test rig. These arches were observed in all the tests.

2.2.3 Failure of the Block Model

The block model was run to complete failure in a model with five layers. The result is shown in Fig. 15. The confinement of the model material was enforced by applying a torque of 2.5 Nm to each bolt on the test frame, which resulted in an estimated confinement of 0.072 MPa. The highest load measured in the test was 9.71 kN with an anchor displacement of 14.1 mm. The load then started to drop gradually with continued displacement. At a displacement of 38.2 mm, the block model completely lost its load-bearing capacity and failed in the form of an inverted cone, as shown in Fig. 15.

3 Numerical Modelling of the Block Model

The block model was re-created in a discontinuous numerical model with the UDEC program (Itasca 2011). The purpose of the numerical model was to verify the observed phenomena in the physical tests, and evaluate the suitability of UDEC for simulating the behaviour of a rock mass subjected to an anchor load. The results from the physical model tests and DIC analysis were used to calibrate the models.

UDEC (Universal Distinct Element Code) software was chosen for the analysis of the block model because of its capabilities to model discontinuous behaviour. The program can model large displacements caused by rigid motion of individual blocks,

by finding the motion through a continuous detection and treatment of the contact between the blocks when solving the equations of motion (Jing 2003), which is ideal when considering the large displacements in the physical tests.

An important parameter in UDEC regarding simulating plastic deformations is computational rounding, as it indirectly simulates the crushing and shearing of block corners. The UDEC manual specifies that the corner rounding should be 1% of the total block length (Itasca 2011). For a 5 cm × 5 cm block, this would result in a rounding radius of 0.5 mm. In the physical tests, it was observed that the crushing of the corners exceeded 0.5 mm and was in multiple locations up to 1–2 cm. The rounding radius had great influence on the displacements in the models, greater than both the joint strength and confinement. Therefore, it was challenging to decide the rounding radius. Based on observations in the physical tests, it was set to 1 mm, but 3 mm was also tested in some models as shown in Table 4.

The numerical block model included two types of materials. The concrete block was a Mohr-Coulomb material with properties determined by the laboratory tests described in Sect. 2.1.2. The frame and the anchor block in the model were made of an elastic steel material with properties of 18-8 grade steel as described by Budynas and Nisbett (2011). The material parameters are presented in Table 2.

There are three types of joints in the UDEC model. The joints between the steel plates or the anchor block and the steel frame had no contact, and therefore the shear strength was set to zero. The cut surfaces of the concrete blocks were smoother than their original surfaces, and were implemented into the model using different friction angles for the original horizontal joints compared to the cut vertical joints. The friction angles of the two types of joint surfaces measured by the tilt tests were implemented as two types of joints in the model. The shear and normal stiffness of the joints are based on best fit from earlier physical tests with eight layers (i.e., tests 1–3 in table 1). The stiffness in the numerical models was found from iterative testing until a satisfactory match was found. The cohesion was set to zero, implying contact joints without infill material. All the joints were considered to be smooth, and therefore the dilation angle is zero (Barton et al. 1985; Kulatilake et al. 2001). The

mechanical properties of the three types of joints are presented in Table 3.

The geometry of the 2D UDEC models was like the physical models; Fig. 16 shows a UDEC model with 8 block layers. The concrete blocks were 5 cm × 5 cm or 2.5 cm × 5 cm in the models. The blocks were placed in a staggered pattern like the physical tests and the number of layers varied. A separate model was also created with 8 layers and continuous joints vertically and horizontally to evaluate the effect of the vertical joints on the arching. The width of the models were 60 cm with two vertical steel plates on the sides. Horizontal forces were applied to the model sides through the vertical steel plates. The anchor loads were applied in the UDEC models under both load and displacement controls. The models were under gravity loading.

3.1 Numerical Modelling Procedure

Several models were set up by varying the number of layers, the corner rounding and the confinement. All simulations followed the following same procedure:

1. The geometry of the model was set up and the outer boundary of the frame was fixed in both x- and y-directions.
2. The model was cycled to equilibrium.
3. Horizontal confinement was applied to the steel plates which were set free to move in the x-direction.
4. It was then cycled to equilibrium again.
5. The steel plates were fixed.
6. The system was then cycled to equilibrium.
7. The anchor block was moved upward in the y-direction to apply the anchor load.
8. The model was then cycled to equilibrium under load control, or it was cycled for a desired time interval under displacement control.

3.2 Numerical Modelling Results

The numerical models gave similar results as the physical tests. The displacements in the rock mass decreased with higher confinements. The numerical models gave smaller displacements at low confinement than the physical models with the same load in the anchor block. Under displacement control, the

load in the numerical models was higher than the physical models for a given displacement except for the models with two and three layers. In the models with two and three layers, the steel plates acted as levers with rotation around the top layer. The results of the numerical models are summarised in Table 4.

3.3 Load Transfer in the UDEC Block Models

The load transfer in the UDEC models started from the anchor block in the bottom of the model. The displacements were largest close to the anchor block in the centre of the model and attenuated to the sides, as shown in Fig. 17. There were similar displacement patterns in the models of both staggered and continuous vertical joints.

The plots of the horizontal stresses in the numerical models showed that compressive load arches were established in the blocks in the same way as was observed in the physical models. Figures 18 and 19 show the horizontal stresses in numerical models with staggered and continuous vertical joints, respectively. In both models, load arches are formed in each layer and the anchor load is transferred to the abutment steel plates through the arches.

4 Discussion

The laboratory tests and discontinuous numerical modelling aimed to develop a better understanding on how the load from a rock anchor affects a layered and jointed rock mass and how such a rock mass would fail. The numerical modelling was used to verify the mechanisms observed and measured in the physical laboratory tests.

The physical tests and numerical models of a block model exposed to an anchor load in small-scale models had similar results. They showed that load bearing arches, voussoir arches, were developed in each layer of the laminated block mass owing to rotations of the blocks within the layer. The test results indicate that load arches may exist in each layer in laminated rock masses if the layer deforms under the anchor load. The load arches transferred the anchor load to the boundaries in the models. In a real rock mass, the load would be transferred to the rock at some distance from the anchor position. Because of the existence of the load arches, the load capacity of the block models

was higher than the weight of the overlying material in the model. As an example, the model with 5-layers had a capacity of 9.71 kN while the estimated capacity with the weight of overlying material was 94 N. The induced horizontal stress from the arches might also have increased the rock mass strength more than what would have been calculated using the rock mass shear strength along the failure surface.

Under the anchor load, the horizontal block layers bulged upwards and separated from each other in a similar way as described by Dados (1984). The block model tests conducted in this paper failed through a combination of sliding, rotation and wedging between the blocks, and at the end in an inverted cone (as shown in Fig. 15). After failure, the blocks in the centre rotated and were lifted, while the blocks on the sides only experienced slight horizontal movement. The failure trajectory followed the joints in a staggered pattern and had a smaller failure angle, approximately 25° , rather than what is used in the design methods, $30\text{--}45^\circ$ (Littlejohn and Bruce 1977). Apparently, the failure shape was affected by the joint pattern in the test.

The total displacement of the anchor block depended on the number of layers and horizontal confinement for a given anchor load. The displacements of the anchor block decrease with increasing confinement for a given anchor load and a constant wall height in the block model, demonstrated in Fig. 10. The displacement of the anchor block with 2 kN loading increased when a constant torque was applied to the side bolts of the model while removing layers from the block model, as shown in Fig. 11. The block model capacity was reduced when the number of layers were reduced. This is demonstrated in Fig. 12,

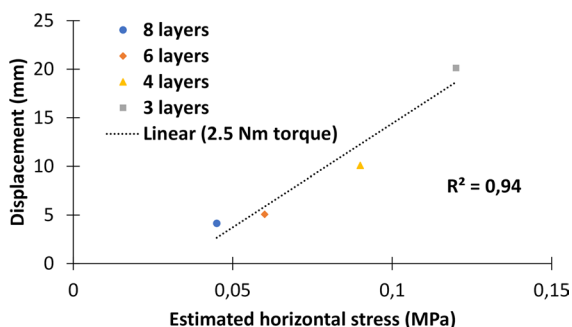


Fig. 11 Vertical displacement at 2 kN anchor load and 2.5 Nm torque applied to side bolts

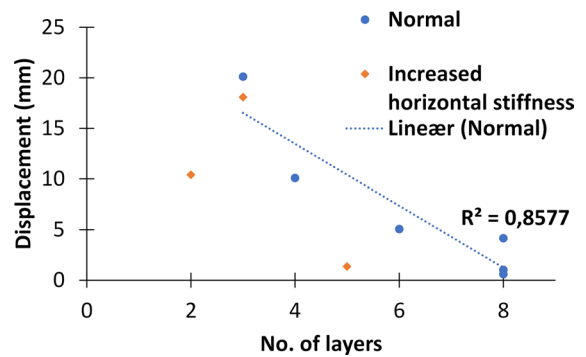


Fig. 12 Vertical displacement at 2 kN anchor load for all the tests under normal conditions with trend line and with increased stiffness of the steel plates

where the vertical displacements increase when the number of layers is reduced at an anchor load of 2 kN.

Figure 12 demonstrates the relationship between the vertical displacement and number of layers. In three of the models the horizontal stiffness was changed, which affected the displacements of the model directly, as can be seen with the orange plotted points. In the final physical test (5 layers) with the smaller steel plates placed in the void between the frame and the steel plates, the increased stiffness resulted in a higher capacity of the physical model compared to earlier tests. These tests indicate that the horizontal stiffness has an effect on the displacements and model capacity; when the stiffness is increased, the displacements decrease. Therefore, it is important to know the stiffness of the material to estimate the displacements and capacity.

These small-scale anchor tests are not direct replications of physical rock anchors. In the model tests, the blocks were loaded by pushing an anchor block upwards, while in reality the anchor is pulled and the load is transferred to the rock mass through the shear stresses along the anchor. The mechanism of the load application in the laboratory tests and the numerical modelling, that is, direct uplift of the blocks above the anchor block, is different from that of the rock anchor in the field, that is, shearing along the bond length of the anchor. This deviation results in different stress fields in a small immediate zone around the anchor. However, the stress distribution further away is not affected. In other words, the load-transferring pattern in the rock mass is not changed significantly by the loading means used in the tests. Therefore,

Table 1 Test parameters and results from the small block model tests

Test no.	No. of block layers	Applied torque (Nm)	Estimated confinement (MPa)	Max. load applied (kN)	Displacement at anchor block (mm)	Load rate (N/s)	Additional comments
1	8	12.5	0.22	5.5	3.4	75	No failure occurred
2	8	7.5	0.13	5.0	7.5	25	No failure occurred
3	8	2.5	0.045	5.0	12.0	21	No material failure observed. However, some cracking could be heard.
4	6	2.5	0.06	5.0	19.0	14	Some spalling in corners of individual blocks, but load capacity of the block stack not exceeded.
5	4	2.5	0.09	3.4	28.0	15	Peak load capacity reached and test stopped.
6	3	2.5	0.12	2.1	31.0	12	Initial failure of block corners at 1.5 kN, peak load capacity reached.
7	2	2.5	0.18	3.0	20.0	27	Peak load capacity reached and test stopped.
8	3	2.5	0.12	2.4	27.0	38	Peak load capacity reached and test stopped.
9	5	2.5	0.072	9.71	38.2	56	Failure of block material and capacity of the stack exceeded.

Fig. 13 Vertical displacement plots (mm) for test 1 at 4 different loads

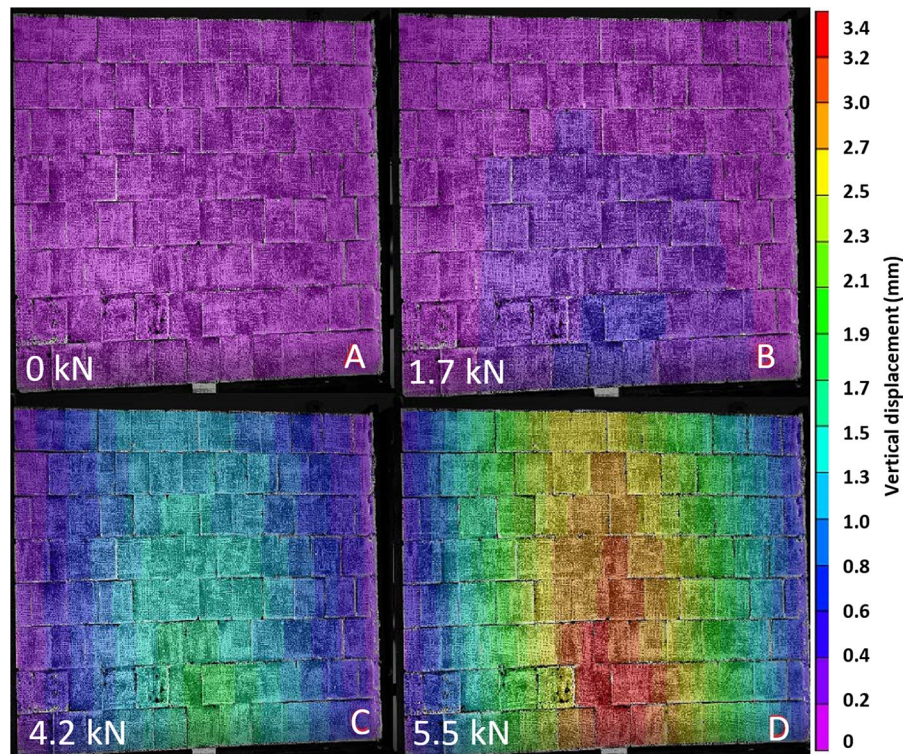


Fig. 14 Plot of the horizontal strain in test 1 with the locations of pressure-transmitting arches drawn in red and potential failure surface based upon the block pattern drawn in yellow

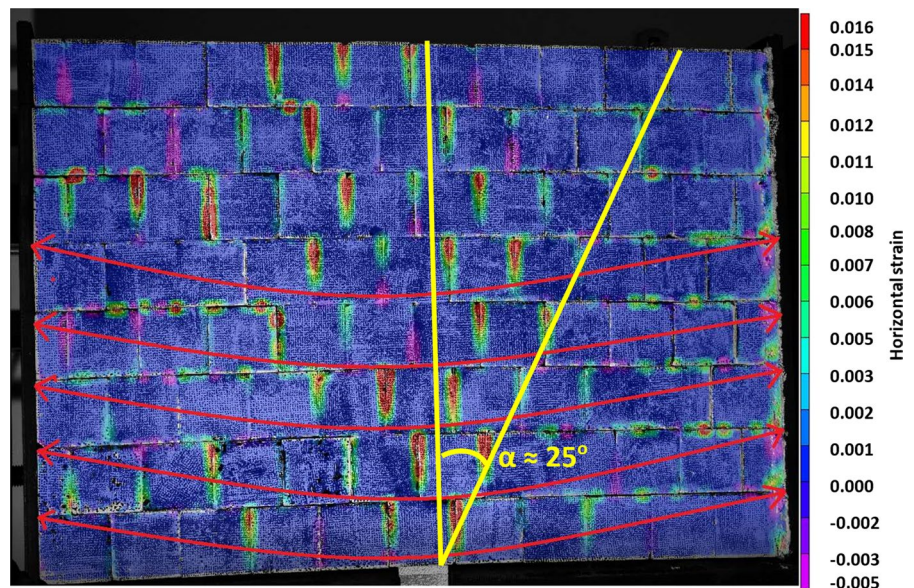


Fig. 15 The model run to failure with 5 layers. The block model failed as an inverted cone

Table 2 Material parameters used in the numerical models

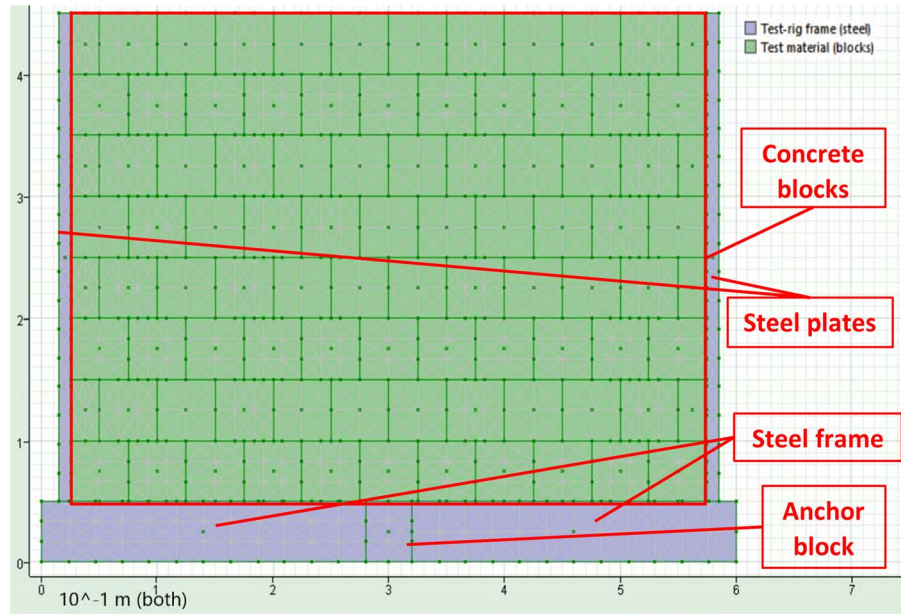
Material	Parameter	Value	Unit
Concrete block material (Mohr-Coulomb)	Density	2300	kg/m ³
	Young's modulus	27.7	GPa
	Poisson's ratio	0.25	
	Friction angle	34	Degrees
Steel frame and anchor block (elastic)	Cohesion	11.2	MPa
	Density	7930	kg/m ³
	Young's modulus	190	GPa
	Poisson's ratio	0.303	

the authors believe that the behaviour presented in this study is a good representative of the behaviour of the rock mass affected by actual rock anchors. Table 4 shows the results of the numerical modelling. The results from the numerical modelling had smaller displacements at the same loads or higher loads at the same displacements as the physical tests. The stiffness in the numerical models was found from iterative testing until a satisfactory match was found. There are several factors that might cause these differences. One likely reason is the difference in the stiffness of the steel plates on the sides of the rock mass in the physical model and the numerical models. The plates are stiffer in the numerical models which prevents the blocks rotating as much as in the physical tests, and the capacity of the block mass is increased. The cement liner used to make all the layers have the same width could be less stiff than the concrete blocks, which may have resulted in more rotation of the blocks in the physical model and a lower capacity than the numerical models.

There are several other factors that might be the cause of the discrepancies between the physical models and the numerical simulations. In the physical model, the contact between the blocks varied since they were cut down to the right size. In some places, it was possible to see through the joints between the blocks while in the numerical model

Table 3 Joint material parameters used in the numerical models

Joint type	Shear stiffness (MPa/m)	Normal stiffness (MPa/m)	Friction angle (degree)	Cohe-sion (MPa)	Dilation angle (degree)	Tension strength (MPa)	Shear disp. at 0 dilation
Concrete vertical joints (cut surface)	1750	3500	31.3	0	0	0	0
Concrete horizontal joints (original block surface)	1750	3500	41.2	0	0	0	0
Steel-steel joints	0	100000	1	0	0	0	0

Fig. 16 Model geometry in UDEC with a staggered block pattern and 8 layers

the contact between the blocks was perfect. Therefore, the contact forces in the numerical models were higher and the block model capacity increased. At high loads in the physical tests, cracking sounds could be heard during testing and the corners of some blocks failed slightly, while in the numerical model the blocks remained intact. The horizontal stress level applied to the numerical models was estimated based on the torque applied to the side bolts on the frame; these estimations are uncertain, and the physical tests and the numerical models showed that the block model displacement was highly influenced by the applied confinement. The estimated confinement was calculated as an average based on the applied torque, while the load distribution possibly was more uneven when there were less than eight layers. In the models with few layers, the steel plates may act as a lever with rotation around

the top layer which results in uneven confinement, which was especially evident in the numerical models with two and three layers.

Further research is needed to evaluate the load arches formed in the rock mass above rock anchors and the failure shape. The joint patterns in the block models should be varied: these tests have only considered continuous horizontal joints and discontinuous vertical joints. Therefore, it would be necessary to test with continuous joints in both directions, joint patterns set at an angle or interlocked joints. The horizontal stress should be measured to evaluate the capacity of the load arches. These results will be used in the development of a large test frame where the confinement can be controlled and measured, and the stresses in the block model determined.

Table 4 Results of numerical simulations of the physical tests

Simulation no. in UDEC/ physical test no. (x/y)	Number of layers	Method, Rounding radius	Applied horizontal stress (MPa)	Applied anchor stress UDEC (MPa)	Measured anchor stress UDEC (MPa)	Equivalent anchor force in physical model (kN)	Displacement anchor block in UDEC (mm)	Displacement anchor block in physical test (mm)
1/1	8	Load controlled, 1.0 mm	0.22	1.4	–	5.6	3.6	3.4
2/2	8	Load controlled, 1.0 mm	0.13	1.3	–	5.2	3.8	7.5
3/3	8	Load controlled, 1.0 mm	0.045	1.3	–	5.2	4.5	12
4/1	8	Load controlled, 3.0 mm	0.22	1.4	–	5.6	4.2	3.4
5/3	8	Load controlled, 3.0 mm	0.045	1.3	–	5.2	5.4	12
6/1	8	Displacement controlled, 1.0 mm	0.022	–	1.45	5.8	3.4	3.4
7/3	8	Displacement controlled, 3.0 mm	0.045	–	3.2	12.8	12	12
8/4	6	Displacement controlled, 3.0 mm	0.06	–	2.2	8.8	19	19
9/- (non staggered blocks)	8	Load controlled, 1.0 mm	0.045	1.7	–	6.8	3.5	–
10/9	5	Displacement controlled, 1.0 mm	0.072	–	1.3	5.2	14	38 (max displacement) 14 (at max load)
11/5	4	Displacement controlled, 1.0 mm	0.09	–	1.5	6.0	28	28
12/6	3	Displacement controlled, 1.0 mm	0.12	–	0.4	1.6	15	31
13/7 (without clamps)	2	Displacement controlled, 1.0 mm	0.18	–	0.32	1.3	20	20

The numbering scheme for the simulations in UDEC is as follows: x/y, where x is the UDEC simulation number and y is the number of the corresponding physical test

5 Conclusion

A series of small-scale two-dimensional block model tests were carried out in the laboratory to investigate load transferring from rock anchor to rock mass. The

test results showed that load transfer arches were formed in individual block layers, through which the anchor load was transferred to the side frames of the test apparatus. The load capacity of the model increased with increases both in the confining stress

Fig. 17 Vertical displacement plot for numerical simulation 1 at equilibrium for a load controlled model with 5.6 kN load of physical test 1

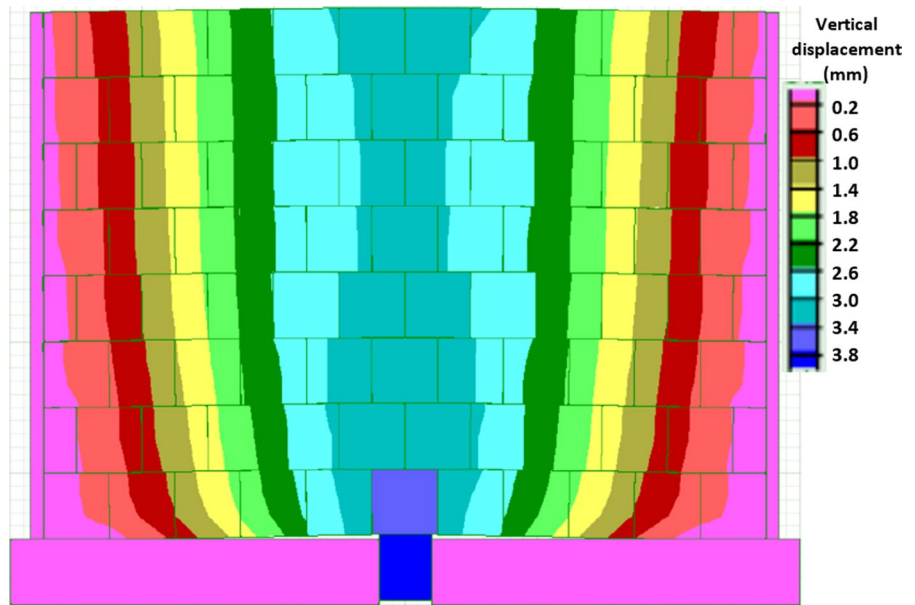
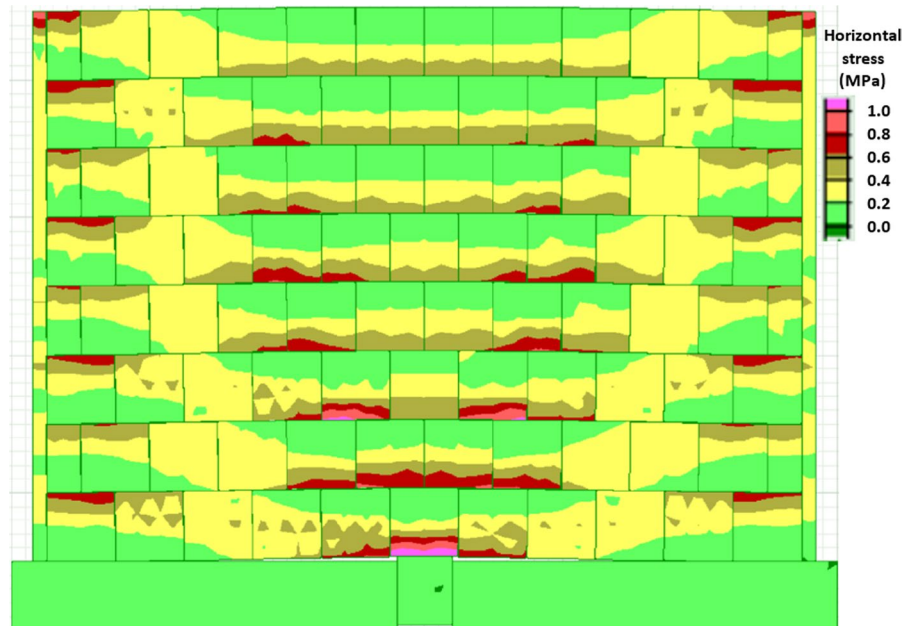


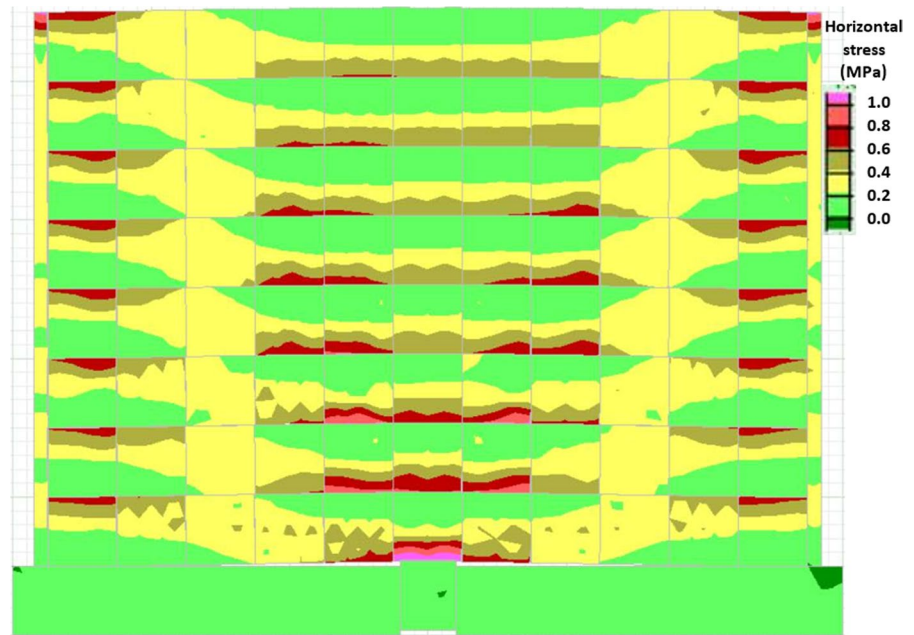
Fig. 18 Horizontal stress plot for numerical simulation 1 with 5.6 kN anchor load for load controlled model of physical test 1



and in the number of block layers (corresponding to an increase in the depth). The trajectory of the inverted failure cone followed the joints in a staggered pattern. The tests also showed that the load capacity of the block model is significantly higher than the weight force of the potential failure cone, which is commonly used to estimate the load capacity of

the rock mass in the current practice of rock anchoring. The observed phenomena like load arching were also captured in the discontinuous UDEC numerical modelling. The numerical modelling revealed that the voussoir arching was achieved owing to block rotations as well as the confinement. The load capacity of the voussoir arches increases with an increase in the

Fig. 19 Horizontal stress plot for numerical simulation 9 at 3.5 mm anchor displacement for a displacement controlled model with a non-staggered block pattern and continuous vertical and horizontal joints



confining stress. The displacements in the mass are approximately identical along a vertical line from the anchor to the ground surface, except in the immediate area surrounding the anchor. At a given depth, the displacement decreases with an increase in the distance to the centre line of the anchor.

Acknowledgements The authors acknowledge the financial support of the Research Council of Norway through the ROCARC research project with project number 303448. The partners of the project are the Norwegian University of Science and Technology (NTNU), SINTEF, NGI, the Arctic University of Norway (UiT), Norwegian Association of Rock Mechanics (NBG), Norwegian Public Roads Administration (NPRA), MultiConsult AS, Norconsult AS, and NORSAR. The authors thank Gunnar Vistnes and Noralf Vedvik for their technical assistance during the laboratory tests.

Author Contributions All authors contributed to the study conception and design. Material preparation, data collection and analysis were performed by Bjarte Grindheim and Karsten Sannes Aasbø. The first draft of the manuscript was written by Bjarte Grindheim and all authors commented on previous versions of the manuscript. All authors read and approved the final manuscript.

Funding Open access funding provided by NTNU Norwegian University of Science and Technology (incl St. Olavs Hospital - Trondheim University Hospital). This work was supported by the Research Council of Norway through the ROCARC research project (project number 303448).

Data Availability The datasets generated during the current study are available from the corresponding author on reasonable request.

Declarations

Conflict of Interest The authors have no relevant financial or non-financial interests to disclose.

Open Access This article is licensed under a Creative Commons Attribution 4.0 International License, which permits use, sharing, adaptation, distribution and reproduction in any medium or format, as long as you give appropriate credit to the original author(s) and the source, provide a link to the Creative Commons licence, and indicate if changes were made. The images or other third party material in this article are included in the article's Creative Commons licence, unless indicated otherwise in a credit line to the material. If material is not included in the article's Creative Commons licence and your intended use is not permitted by statutory regulation or exceeds the permitted use, you will need to obtain permission directly from the copyright holder. To view a copy of this licence, visit <http://creativecommons.org/licenses/by/4.0/>.

References

- Akisanya AR, Ivanovic A (2014) Debonding along the fixed anchor length of a ground anchorage. *Eng Struct* 74:23–31. <https://doi.org/10.1016/j.engstruct.2014.05.013>
- Alejano LR, Muralha J, Li CC et al (2018) ISRM suggested method for determining the basic friction angle of

- planar rock surfaces by means of tilt tests. *Rock Mech Rock Eng* 51:3853–3859. <https://doi.org/10.1007/s00603-018-1627-6>
- Aoki K (2007) Design and construction of large rock caverns supported by ground anchorages. In: *Ground Anchorages and Anchored Structures in Service*. In: *Proceedings of the International Conference*. Thomas Telford Publishing, London, pp 188–198
- Barley AD (1997) Properties of anchor grouts in a confined state. In: *Ground Anchorages and Anchored Structures: Proceedings of the International Conference*. Thomas Telford Publishing, London, England, pp 371–383
- Barton N, Bandis S, Bakhtar K (1985) Strength, deformation and conductivity coupling of rock joints. *Int J Rock Mech Min Sci Geomech Abstr* 22(3):121–140. [https://doi.org/10.1016/0148-9062\(85\)93227-9](https://doi.org/10.1016/0148-9062(85)93227-9)
- Benmokrane B, Chekired M, Xu H (1995) Monitoring behavior of grouted anchors using vibrating-wire gauges. *J Geotech Eng* 121(6):466–475. [https://doi.org/10.1061/\(ASCE\)0733-9410\(1995\)121:6\(466\)](https://doi.org/10.1061/(ASCE)0733-9410(1995)121:6(466))
- Benmokrane B, Chennouf A, Mitri HS (1995) Laboratory evaluation of cement-based grouts and grouted rock anchors. *Int J Rock Mech Min Sci Geomech Abstr* 32(7):633–642. [https://doi.org/10.1016/0148-9062\(95\)00021-8](https://doi.org/10.1016/0148-9062(95)00021-8)
- Bieniawski Z, Bernede M (1979) Suggested methods for determining the uniaxial compressive strength and deformability of rock materials. *Int J Rock Mech Min Sci Geomech Abstr* 16(2):137–140. [https://doi.org/10.1016/0148-9062\(79\)91451-7](https://doi.org/10.1016/0148-9062(79)91451-7)
- Brown ET (2015) Rock engineering design of post-tensioned anchors for dams—a review. *J Rock Mech Geotech Eng* 7(1):1–13. <https://doi.org/10.1016/j.jrmge.2014.08.001>
- Budynas RG, Nisbett JK (2011) *Shingley's Mechanical Engineering Design* -, 9th edn. McGraw-Hill, New York, USA
- Cavill BA (1997) Very high capacity ground anchors used in strengthening concrete gravity dams. In: *Ground Anchorages and Anchored Structures: Proceedings of the International Conference*. Thomas Telford Publishing, London, England, pp 262–271
- Choi SW, Lee J, Kim JM et al (2013) Design and application of a field sensing system for ground anchors in slopes. *Sensors* 13(3):3739–3752. <https://doi.org/10.3390/s130303739>
- Correlated Solutions (2020) *Vic-3D v7 Testing Guide*. Correlated Solutions
- Dados AT (1984) Design of anchors in horizontally jointed rocks. *J Geotech Eng* 110(11):1637–1647. [https://doi.org/10.1061/\(ASCE\)0733-9410\(1984\)110:11\(1637\)](https://doi.org/10.1061/(ASCE)0733-9410(1984)110:11(1637))
- Farmer IW (1975) Stress distribution along a resin grouted rock anchor. *Int J Rock Mech Min Sci Geomech Abstr* 12(11):347–351. [https://doi.org/10.1016/0148-9062\(75\)90168-0](https://doi.org/10.1016/0148-9062(75)90168-0)
- García-Wolfrum S, Serrano A, Olalla C (2007) Model failure tests on rock anchors. 11th Congr Int Soc Rock Mech Second Half Century Rock Mech. Taylor & Francis Group, Lisbon, Portugal, ISRM, pp 339–342
- Hanna TH (1982) *Foundations in tension: ground anchors*. Trans Tech Publications and McGraw-Hill Book Company, Clausthal, Germany
- Hobst L, Zajíc J (1983) *Anchoring in Rock and Soil*. Elsevier Scientific Publishing Company, New York, USA
- Standard Indian (2000) IS 456:2000 - Plain and reinforced concrete - code of practice (fourth revision). Bureau of Indian Standards, New Delhi, India
- Itasca, (2011) UDEC 50 user manual. Itasca Consulting Group Inc., Minneapolis
- Ivanovic A, Neilson RD (2008) Modelling of debonding along the fixed anchor length. *Int J Rock Mech Min Sci* 46(4):699–707. <https://doi.org/10.1016/j.ijrmmms.2008.09.008>
- Jarred DJ, Haberfield CM (1997) Tendon/grout interface performance in grouted anchors. In: *Ground Anchorages and Anchored Structures: Proceedings of the International Conference*. Thomas Telford Publishing, London, England, pp 3–12
- Jia J, Li B, Liu F (2019) Experimental study on mix proportion parameter optimization of cement anchoring material. *Materials* 13(1):22. <https://doi.org/10.3390/ma13010137>
- Jing L (2003) A review of techniques, advances and outstanding issues in numerical modelling for rock mechanics and rock engineering. *Int J Rock Mech Min Sci* 40(3):283–353. [https://doi.org/10.1016/S1365-1609\(03\)00013-3](https://doi.org/10.1016/S1365-1609(03)00013-3)
- Jordan L (2007) Monitoring of multi-strand ground anchors at the city of Manchester stadium. In: *Ground Anchorages and Anchored Structures in Service*. In: *Proceedings of the International Conference*. Thomas Telford Publishing, London, England, pp 99–110
- Kaiser PK, Yazici S, Nosé J (1992) Effect of stress change on the bond strength of fully grouted cables. *Int J Rock Mech Min Sci Geomech Abstr* 29(3):293–306. [https://doi.org/10.1016/0148-9062\(92\)93662-4](https://doi.org/10.1016/0148-9062(92)93662-4)
- Kim DH, Lee SR (2005) Uplift capacity of fixed shallow anchors subjected to vertical loading in rock. *Int J Offshore Polar Eng* 15(4):312–320
- Kim HK, Cho NJ (2012) A design method to incur ductile failure of rock anchors subjected to tensile loads. *Electron J Geotech Eng* 17:2737–2746
- Koca MY, Kincal C, Arslan AT et al (2011) Anchor application in Karatepe andesite rock slope, Izmir - Türkiye. *Int J Rock Mech Min Sci* 48(2):245–258. <https://doi.org/10.1016/j.ijrmmms.2010.11.006>
- Kulatilake PHSW, Liang J, Gao H (2001) Experimental and numerical simulations of jointed rock block strength under uniaxial loading. *J Eng Mech* 127(12):1240–1247. [https://doi.org/10.1061/\(ASCE\)0733-9399\(2001\)127:12\(1240\)](https://doi.org/10.1061/(ASCE)0733-9399(2001)127:12(1240))
- Littlejohn GS, Bruce DA (1977) *Rock anchors - state of the art*. Foundation publications Ltd., Brentwood, Essex, England
- Ma Y, Su C (2020) Zhang H (2021) Analysis of surrounding rock anchoring effect under the condition of squeezed mountain. IOP Conference Series: Earth and Environmental Science 669. IOP Publishing, Zhengzhou, China, ICSSCER, p 10
- Mothersille D, Littlejohn S (2012) Grouting of anchors to resist hydrostatic uplift at Burnley tunnel, Melbourne, Australia. In: *Proceedings of the Fourth International Conference on Grouting and Deep Mixing*. American Society of Civil Engineers, New Orleans, Louisiana, USA, GSP, pp 1073–1084
- Park J, Qiu T, Kim Y (2013) Field and laboratory investigation of pullout resistance of steel anchors in rock. *J Geotech*

- Geoenviron Eng 139(2):2219–2224. [https://doi.org/10.1061/\(ASCE\)GT.1943-5606.0000953](https://doi.org/10.1061/(ASCE)GT.1943-5606.0000953)
- Roesen BS, Trankjær H (2021) Permanent uplift anchors in Copenhagen limestone. In: IOP Conference Series: Earth and Environmental Science 710. IOP Publishing, Helsinki, Finland, 18th Nordic Geotechnical Meeting, p 10
- Schlotfeldt P, Panton B, Humphries R, et al (2013) New Park Bridge, Kicking Horse Canyon; Pier 5 - A difficult foundation on rock. In: 47th US Rock Mechanics/ Geomechanics Symposium. American Rock Mechanics Association, San Francisco, California, USA, p 8
- Shabanimashcool M, Olsson R, Valstad T, et al (2018) Numerical modelling of anchored foundation for wind turbine generators, WTG (in Norwegian). In: Fjellsprengningsdagen - Bergmekanikkdagen - Geoteknikkdagen. NFF, NBG, NGF, Oslo, Norway, Bergmekanikkdagen, pp 18.1–18.24
- Showkati A, Maarefvand P, Hassani H (2015) Stress induced by post-tensioned anchor in jointed rock mass. J Central South Univ 22:1463–1476. <https://doi.org/10.1007/s11771-015-2664-x>
- Sivakugan N, Das BM, Lovisa J et al (2014) Determination of c and ϕ of rocks from indirect tensile strength and uniaxial compression tests. Int J Geotech Eng 8(1):59–65. <https://doi.org/10.1179/1938636213Z.00000000053>
- Takemura J, Kubo H, Yamazaki J (2007) Field surveys of anchored slopes after 2004 Niigataken Chuetsu earthquake. In: Ground Anchorages and Anchored Structures in Service, Proceedings of the International Conference. Thomas Telford Publishing, London, England, pp 407–416
- Tu H, Zhou H, Lu J et al (2020) Elastoplastic coupling analysis of high-strength concrete based on tests and the Mohr-Coulomb criterion. Constr Build Mater 255:119375. <https://doi.org/10.1016/j.conbuildmat.2020.119375>
- USACE (1990) Military handbook: Threaded fasteners - tightening to proper tension. Tech. Rep. MIL-HDBK-60, U.S. Department of Defense, Washington DC, USA
- Wang HT, Zhang XH, He Y et al (2018) Field measurement and numerical simulation analysis of high and steep slope reinforced by prestressed anchor. IACGE 2018: Geotechnical and Seismic Research and Practices for Sustainability. ASCE, Chongqing, China, IACGE, pp 123–135
- Xanthakos PP (1991) Ground anchors and anchored structures. Wiley, New York
- Xu H, Benmokrane B (1996) Strengthening of existing concrete dams using post-tensioned anchors: a state-of-the-art review. Can J Civil Eng 23(6):1151–1171. <https://doi.org/10.1139/196-925>
- Yan S, Song BC, Sun W, et al (2013) Stress state analysis on a rock anchor RC foundation of wind driven generator. In: The 2013 World Congress on Advances on Structural Engineering and Mechanics. Daejeon Techno-Press, Jeju, Korea, ASEM13, pp 2202–2213
- Zheng D, Liu FZ, Ju NP et al (2016) Cyclic load testing of pre-stressed rock anchors for slope stabilization. J Mt Sci 13:126–136. <https://doi.org/10.1007/s11629-015-3605-8>

Publisher's Note Springer Nature remains neutral with regard to jurisdictional claims in published maps and institutional affiliations.